POTSDAM-INSTITUT FÜR
KLIMAFOLGENFORSCHUNG

Reconstructing the last interglacial at Summit, Greenland: Insights from GISP2

Audrey M. Yau[a], Michael L. Bender[a,b,1], Alexander Robinson[c,d,e], and Edward J. Brook[f]

[a]Department of Geosciences, Princeton University, Princeton, NJ 08540; [b]Institute of Oceanology, Shanghai Jiao Tong University, Minhang District, Shanghai 200240, China; [c]Universidad Complutense de Madrid, 28040 Madrid, Spain; [d]Instituto de Geociencias, Universidad Complutense de Madrid–Consejo Superior de Investigaciones Científicas, 28040 Madrid, Spain; [e]Potsdam Institute for Climate Impact Research, 14473 Potsdam, Germany; and [f]College of Earth, Ocean, and Atmospheric Sciences, Oregon State University, Corvallis, OR 97331

Edited by Jeffrey P. Severinghaus, Scripps Institution of Oceanography, La Jolla, CA, and approved June 17, 2016 (received for review December 16, 2015)

The Eemian (last interglacial, 130–115 ka) was likely the warmest of all interglacials of the last 800 ka, with summer Arctic temperatures 3–5 °C above present. Here, we present improved Eemian climate records from central Greenland, reconstructed from the base of the Greenland Ice Sheet Project 2 (GISP2) ice core. Our record comes from clean, stratigraphically disturbed, and isotopically warm ice from 2,750 to 3,040 m depth. The age of this ice is constrained by measuring CH_4 and $\delta^{18}O$ of O_2, and comparing with the historical record of these properties from the North Greenland Ice Core Project (NGRIP) and North Greenland Eemian Ice Drilling (NEEM) ice cores. The $\delta^{18}O_{ice}$, $\delta^{15}N$ of N_2, and total air content for samples dating discontinuously from 128 to 115 ka indicate a warming of ∼6 °C between 127–121 ka, and a similar elevation history between GISP2 and NEEM. The reconstructed climate and elevation histories are compared with an ensemble of coupled climate-ice-sheet model simulations of the Greenland ice sheet. Those most consistent with the reconstructed temperatures indicate that the Greenland ice sheet contributed 5.1 m (4.1–6.2 m, 95% credible interval) to global eustatic sea level toward the end of the Eemian. Greenland likely did not contribute to anomalously high sea levels at ∼127 ka, or to a rapid jump in sea level at ∼120 ka. However, several unexplained discrepancies remain between the inferred and simulated histories of temperature and accumulation rate at GISP2 and NEEM, as well as between the climatic reconstructions themselves.

Greenland ice sheet | last interglacial | ice cores | sea level rise

During the last interglacial (Eemian, 130–115 ka), Arctic summer temperatures were 3–5 °C warmer than today (1), and peak global eustatic sea level was likely 6–9 m higher than the present (2). In the next century, due to anthropogenic emissions of greenhouse gases, we face a similar temperature scenario with 2–6 °C of northern hemispheric polar warming (3), and a likely initial sea level rise (by 2100) of 0.3–1.0 m (4), with higher, but uncertain, levels beyond. Certainly there are important differences between the warming and sea level change observed during the last climatic warm period and future projections, notably the rate at which warming is expected to occur and its spatial pattern. Nevertheless, the Eemian history of the Greenland ice sheet (GrIS) serves as an essential test bed for understanding changes in ice sheets and sea level rise in response to rising global temperatures.

Ice sheet modeling studies have estimated a wide range of GrIS contributions to sea level during the Eemian, with simulations producing 0.4–5.5 m of equivalent sea level rise above the present datum (5). Although ice dating to the Eemian or beyond has been observed in six ice cores drilled to the base of the Greenland ice sheet [North Greenland Ice Core Project (NGRIP), GRIP, Greenland Ice Sheet Project 2 (GISP2), Camp Century, Dye 3, and North Greenland Eemian Ice Drilling (NEEM)] (Fig. 1), only the most recently drilled core at NEEM has provided a continuous climate history through the Eemian, with ice as old as 128 ka (6). The NEEM climate record includes data on gas stratigraphy (which defines the timescale), isotopic temperature, gas-trapping depth (from $\delta^{15}N$ of N_2), and total air content (7).

Here, we revisit the climate archive of the deep section of the GISP2 ice core, which contains stratigraphically disturbed layers of ice dating to the last interglacial and beyond (8, 9). The GISP2 ice core was drilled to bedrock in 1993, producing a 3,053.44-m ice core at Summit, Greenland. Its stratigraphy is continuous to only ∼105 ka, or to a depth of ∼2,750 m (Fig. 1). Below, there are ∼290 m with alternating intervals of isotopically warm (heavy $\delta^{18}O_{ice}$) and cold (light $\delta^{18}O_{ice}$) ice (10). The warmest of these sections have $\delta^{18}O_{ice}$ values warmer than that of the current interglacial, and gas properties consistent with an Eemian age, indicating that Eemian ice is present near the bed of GISP2 (Fig. 1; refs. 9, 11).

We targeted the warmest disturbed ice, sampling all 48 one-meter sections of the GISP2 ice core between 2,760 and 3,040 m depth with $\delta^{18}O_{ice}$ values heavier than –37‰ (Fig. S1). Measurements of the $\delta^{18}O$ of paleoatmospheric O_2 ($\delta^{18}O_{atm}$) and the concentration of CH_4 constrain the ages of discrete samples. We then use these dates to improve our understanding of the sequence of events at Summit, Greenland, during the last interglacial. The product is a discontinuous record of isotopic temperatures and ice accumulation rates, as well as the elevation of GISP2 with respect to NEEM, over the Eemian at Summit, Greenland. Finally, we compare model simulations to the reconstructed GISP2 and NEEM records to estimate the regional climatic change and sea level contribution from the GrIS during the Eemian.

Age Reconstruction

To establish a chronology for the sampled sections, we follow earlier work in measuring the $\delta^{18}O$ of paleoatmospheric oxygen ($\delta^{18}O_{atm}$), and the concentration of CH_4, in the trapped air bubbles in the ice (8, 9). Throughout the global atmosphere, $\delta^{18}O_{atm}$ and CH_4 each vary with time, more or less uniformly. We date disturbed ice by determining when, according to existing

Significance

This work contributes to the scientific effort focused on developing an accurate assessment of the impact that global warming will have on the Greenland ice sheet. By focusing on the last interglacial, a period warmer than today, we learn about the sensitivity of the ice sheet to climate change. We combine data and model simulations to characterize the Eemian history of the Greenland ice sheet. Our data and insights will be useful for simulating the future of the ice sheet in response to climate change.

Author contributions: A.M.Y. and M.L.B. designed research; A.M.Y. performed research; E.J.B. contributed new reagents/analytic tools; A.M.Y., M.L.B., A.R., and E.J.B. analyzed data; and A.M.Y., M.L.B., and A.R. wrote the paper.

The authors declare no conflict of interest.

This article is a PNAS Direct Submission.

[1]To whom correspondence should be addressed. Email: bender@princeton.edu.

This article contains supporting information online at www.pnas.org/lookup/suppl/doi:10.1073/pnas.1524766113/-/DCSupplemental.

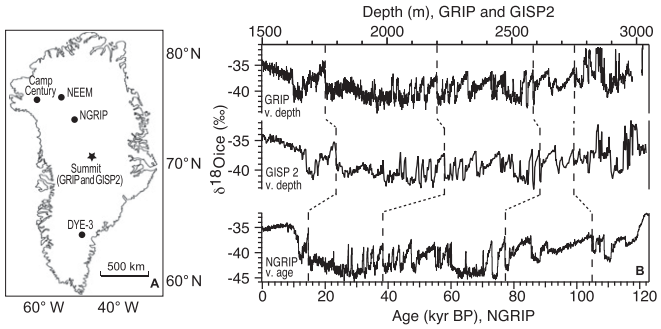

Fig. 1. (*A*) Relevant Greenland ice core drilling sites. (*B*) Comparison of $\delta^{18}O_{ice}$ for GRIP, GISP2, and NGRIP ice cores (10, 11). GRIP and GISP2 are plotted on the top axis vs. depth and are continuous to ∼2,750 m. NGRIP is plotted on the bottom axis vs. age and is continuous to ∼121 ka. Dotted lines show $\delta^{18}O_{ice}$ correlations between cores.

Greenland and Antarctic ice core records, the atmosphere had the same CH_4 concentration and $\delta^{18}O_{atm}$ we observe in a particular sample (Fig. 2 and Fig. S2). The following ice core records provide the reference $\delta^{18}O_{atm}$ and CH_4 stratigraphy: NGRIP from 121.1 to 105 ka (12); NEEM from 128.2 to 119.9 ka [ref. 6; EPICA Dronning Maud Land (EDML1) gas age timescale]; and European Project for ice coring in Antarctica (EPICA) Dome C, dated continuously to ∼800 ka (refs. 13, 14; Antarctic Ice Core Chronology 2012 gas age timescale). In the NEEM dataset, samples with elevated CH_4 and N_2O concentrations are associated with melt layers, and are removed from the reference curve (ref. 6; Fig. S3). Our analysis dates ice at 28 depths in the GISP2 core between 116 and 128 ka. Details are given in the *Supporting Information*.

Coupled Climate–Ice-Sheet Model

The coupled climate–ice-sheet model approach, Regional Energy-Moisture Balance - Simulation Code for Polythermal Ice Sheets (REMBO-SICOPOLIS), was used to simulate the evolution of the GrIS through the Eemian. Regional climatic conditions over Greenland and the surface mass balance are calculated by the intermediate complexity regional climate model REMBO (15). REMBO includes a computationally efficient 2D atmospheric component and a simplified energy-balance model for calculating the surface mass balance of the ice sheet. The evolution of the ice sheet is calculated via the 3D thermomechanical, shallow-ice approximation ice sheet model SICOPOLIS (16). SICOPOLIS is driven by the ice surface temperature and surface mass balance fields calculated in REMBO, and in turn it provides ice sheet thickness and elevation as topographic input back to REMBO. The coupled model is run at 20-km resolution, and it has been shown to simulate the volume and distribution of the present-day ice well (16). Importantly for this study, the model accounts for the albedo–temperature and elevation–melt feedbacks that are active in times of transient ice sheet evolution, such as during the Eemian. REMBO is driven at the boundaries by monthly temperature anomalies around Greenland, computed using the CLIMBER-2 earth system model of intermediate complexity in a global glacial cycle simulation from 860 ka to the present driven by greenhouse gas forcing and Milankovitch variability (17).

An ensemble of simulations was performed through the Eemian accounting for parametric uncertainty associated with the melt model and the sensitivity of precipitation to temperature changes (18), which are dominant factors affecting the transient evolution of the ice sheet. In addition, the positive monthly temperature anomalies during the Eemian were scaled by a random factor to test a wide range of interglacial temperatures. The ensemble was generated using Latin hypercube sampling, where the parameter values were perturbed within a range consistent with present-day constraints (18), and the interglacial temperature anomalies were perturbed to give a peak summer warming range of between approximately 1 and 6 °C. Prior estimates of parameter weights were assigned to each model version and a posterior likelihood of each simulation was obtained by statistical comparison between the modeled and reconstructed precipitation-weighted temperature anomalies at GISP2 and the NEEM deposition site (see *Supporting Information* for details).

Results and Discussion

Climate at Summit, Greenland, over the Last Interglacial. Fig. 3 shows climate properties for samples from the clean, disturbed section of the GISP2 core plotted vs. reconstructed age. Also plotted are similar GISP2 data of Suwa et al. (8), along with the reconstructed records from NEEM (6). We note that temperature reconstructions are based on precipitation-weighted $\delta^{18}O_{ice}$, which is likely biased toward warmer summer months rather than the annual mean temperature (19).

Temperature. We observe a rapid deglacial warming at Summit, similar to that seen in the NEEM core. From 127.6 to 126.6 ka, GISP2 $\delta^{18}O_{ice}$ increases by 2.9‰ from −35.2‰ to −32.3‰ (Fig. 3*A*). To estimate temperatures, we adopt the temperature–$\delta^{18}O$ relationship of Vinther et al. (20), with the larger uncertainty of *NEEM* (6), i.e., $dT/d\delta^{18}O_{ice} = 2.1 \pm 0.5$ °C ‰$^{-1}$. This value is similar to the present-day spatial relationship of $\delta^{18}O_{ice}$ vs. temperature, 1.5 °C ‰$^{-1}$ (21). The $dT/d\delta^{18}O$ relationship may differ between the Eemian and the Holocene due to changes in seasonality and sources of precipitation (19), as well as topographic feedbacks with a reduced ice sheet size (22), which is reflected in the uncertainty range used here. Using this conversion factor, the $\delta^{18}O_{ice}$ change corresponds to a precipitation-weighted warming of 6 ± 1.5 °C at Summit over an ∼1,000-y period. After a plateau of several kiloyears, $\delta^{18}O_{ice}$ gradually decreases by ∼1.5‰ from 121.8 to 118 ka, corresponding to a cooling of 3 ± 1 °C, again, much like that seen at NEEM.

During the middle of the Eemian, $\delta^{18}O_{ice}$ at GISP2 is slightly lower than at NEEM, suggesting that the Summit anomaly was perhaps 1 °C lower. At NEEM, highly variable total air content data, along with sharp spikes in CH_4 and N_2O concentrations, indicate frequent surface melt layers between 128 and 118 ka (6). Such features are not observed at GISP2. Unfortunately, our ability to describe this interval at GISP2 is limited by the paucity of GISP2 and GRIP samples dating between 126 and122 ka (this work; ref. 8), which notably corresponds to the period of warmest Eemian temperatures and significant Greenland ice sheet loss (6).

The reconstructed temperature anomaly relative to the mean of the last thousand years is calculated and plotted in Fig. 3*B*. For reference, present-day values of $\delta^{18}O_{ice}$ and temperature are −35‰ and −31 °C for GISP2 and −35‰ and −29 °C for the

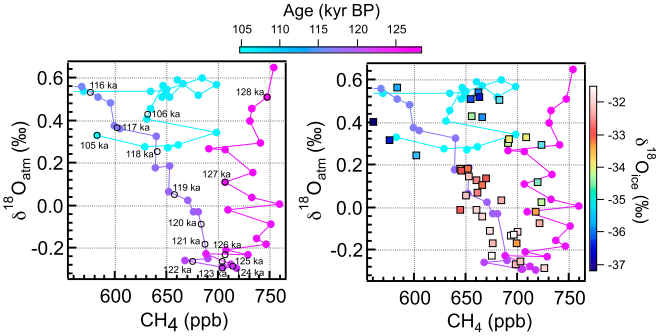

Fig. 2. Reference curves of CH_4 vs. $\delta^{18}O_{atm}$ color-coded for age. (*A*) Reference curve based on NGRIP (121.1–105 ka; 12) and NEEM (128.2–119.9 ka; 6) CH_4 and $\delta^{18}O_{atm}$ data. (*B*) Analyzed sample sections plotted as squares, color-coded for $\delta^{18}O_{ice}$ on the reference curve from *A*.

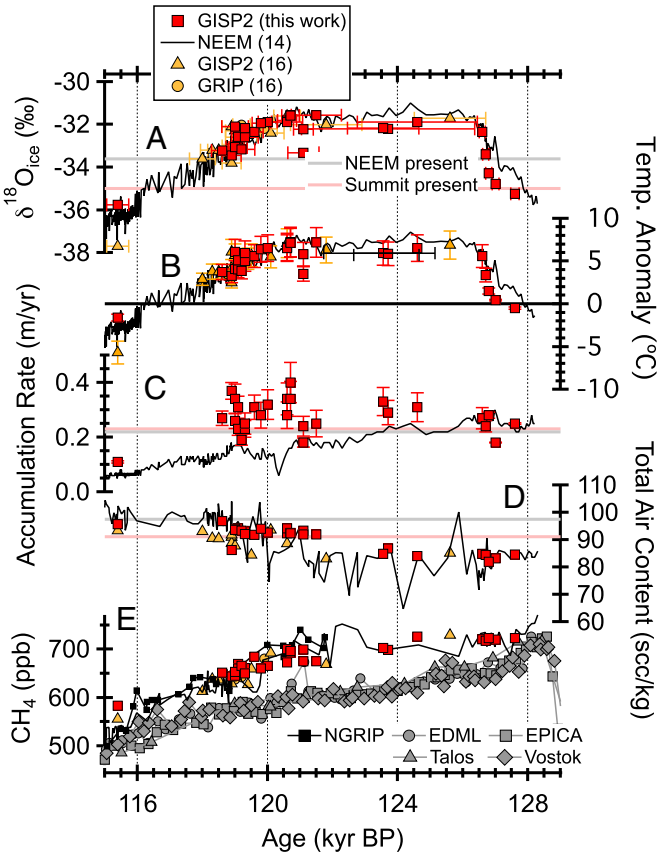

Fig. 3. Summary of data from GISP2 (present study) in red, GRIP and GISP2 in orange (8), and NEEM in black (6) through the last interglacial. (*A*) Reconstructed $\delta^{18}O_{ice}$. (*B*) Calculated temperature anomaly relative to the mean of the last millennium for a $dT/d\delta^{18}O$ relationship of 2.1 ± 0.5 °C ‰$^{-1}$ (6). (*C*) Estimated accumulation rate. (*D*) Reconstructed total air content. (*E*) A comparison of CH_4 data from GISP2 (present study), GRIP and GISP2 (8), NEEM (6), NGRIP (12), EDML (28), EPICA Dome C (13), Talos (29), and Vostok (30).

estimated upstream Eemian NEEM deposition site (6), respectively. Between 126 and 122 ka, Summit temperatures are estimated to have been 4–8 °C higher than the recent average. This warming reflects the combination of higher regional temperatures and lower ice sheet elevation.

Accumulation rate. We calculate the accumulation rate as described in the *Supporting Information*. In brief, we calculate temperature from $\delta^{18}O_{ice}$ as described above. Next, we calculate gas-trapping depth from $\delta^{15}N$ of N_2 (23). The equations of Herron and Langway (24) are then solved to calculate the accumulation rate, in units of water-equivalent meters/year, accounting for close off at the observed temperature and gas-trapping depth. Estimated accumulation rates are shown in Fig. 3*C*. Accumulation rates decline steadily through the Eemian at NEEM, although they are more variable and do not show a trend at GISP2. Accumulation rates are similar between the two sites at the onset and end of the interglacial period, but reach lower values at NEEM by ~120 ka.

Total air content and elevation. The change in total air content (TAC) at GISP2 is easily quantified. However, at NEEM, the situation is complicated by melting, which leads to anomalously low total air content in many of the samples. The reliable TAC values at NEEM are the highest values except for one anomalously high point at 126 ka. These values are very similar to values at GISP2 throughout the record (Fig. 3*D*).

In principle, TAC serves as a proxy for elevation. The premise is that, in ice reaching the close-off depth, open porosity is a function of temperature (7, 25). TAC is then the open porosity at the close-off depth multiplied by the temperature-dependent density of air. Reversing the approach, one can calculate atmospheric pressure during gas trapping from temperature ($\delta^{18}O_{ice}$), the empirical relationship between close-off volume and temperature, and the ideal gas law. In addition, Raynaud et al. (7) and others (26, 27) identified a link between total air content and local summertime insolation. Accounting for this link, NEEM et al. (6) quantified the effect of insolation and estimated that, during the Eemian, elevation at NEEM was within a few hundred meters of the present elevation.

The similarity in TAC at NEEM and GISP2 is at least partly due to the fact that the insolation change is nearly identical at these sites. However, the similarity in the records also requires that the magnitude of elevation change between 127 and 121 ka be similar at the two sites. We have less confidence in absolute elevations computed from the TAC data (*Supporting Information*), because of the large uncertainty associated with the insolation effect as well as the potential for unquantified regional atmospheric pressure changes. Therefore, they are not considered in our analysis.

In summary, GISP2 data place three important constraints on the history of the Greenland ice sheet. First, Summit warmed to the present temperature at ~127 ka, and was ~5 °C warmer than present between 126 and 120 ka. Second, Eemian accumulation rates at Summit were ~40% higher than during the Holocene. Third, the elevation and temperature difference between Summit and the deposition site of NEEM was approximately constant during the Eemian.

Data–Model Comparison. We compare output from an ensemble of coupled climate–ice sheet model simulations to the reconstructed temperature, accumulation rate, and elevation change data for Summit and the NEEM upstream deposition location during the Eemian.

Several simulations capture either the GISP2 or the NEEM temperature record fairly well, but it is not possible to simulate both well simultaneously (Fig. 4). The basic problem is that the NEEM–GISP2 elevation difference should not change appreciably according to TAC data and the isotopic temperature difference between sites. In our simulations, however, NEEM always declines in elevation more than GISP2, and its isotopic temperature increases more. Given our inability to simultaneously simulate climate records at both sites, we derive histories of temperature and elevation by independently optimizing properties of the model to fit the NEEM and GISP2 temperature histories.

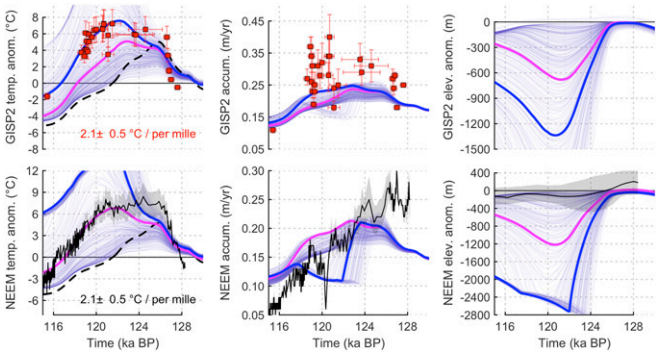

Fig. 4. Simulation output (light-blue lines) of the local precipitation-weighted temperature anomaly (*Left*), the accumulation rate (*Center*), and the elevation (*Right*) compared with reconstructions at GISP2 (*Upper*, in red) and NEEM (*Lower*, in black; gray shading represents SE). The most likely simulations compared with the GISP2 (thick blue lines) and NEEM (thick magenta lines) temperature reconstructions are shown, along with the respective regional summer temperature anomaly forcing in *Left* (dashed black lines).

The optimal simulation accounting only for the GISP2 temperature reconstruction (Fig. 4, blue lines) produces a peak sea level contribution from the GrIS of 6 m (Fig. 5). The trajectory of warming during the Eemian is well captured by the simulation, aside from an underestimation of warming early on of ∼2 °C. It is interesting to note that the model fits the data best toward the end of the interglacial when the combination of transient elevation changes and regional climatic forcing leave the model with the most degrees of freedom (Fig. 6). In this case, the ice sheet is reduced to a small central dome with a reduction in the GISP2 elevation by around 1,300 m (Fig. 6, *Top*). This solution seems to fail because it predicts the absence of an Eemian ice sheet at the NEEM deposition site inferred by ref. 6.

The optimum solution using the NEEM reconstruction (Fig. 4, magenta lines) still gives a rather large peak sea level contribution of 5 m (Fig. 5). As with the GISP2-optimal simulation, the initial warming entering the Eemian is underestimated by ∼3 °C, and the simulation matches the later trajectory of the reconstruction quite well. This simulation implies an elevation reduction of approximately 1,200 m relative to today at the NEEM deposition site, and a much smaller reduction in elevation at GISP2 of only 700 m (Fig. 5, *Bottom Right*). This solution also seems deficient. It fails to simulate the constant elevation difference between NEEM and GISP2. It also underestimates the temperature anomaly at GISP2 by 3 ± 1 °C between 119 and 123 ka.

The estimated peak regional summer warming (black dashed lines in Fig. 4, prescribed as boundary forcing in the regional climate model) is quite similar in both cases. The combined GISP2 and NEEM posterior likelihood using this forcing gives a best estimate of ∼4.5 °C regional summer warming, and a 95% credible interval of 3–5 °C. This range is quite consistent with previous best estimates of Arctic summer warming during this time period (1). The optimal solutions are also consistent in placing the greatest sea level contribution late in the Eemian, at ∼121 ka (Fig. S4), which is also when the regional summer temperature falls below the modern value in the simulations. At its minimum, the resulting GrIS is reduced to a rather small northern dome and some sporadic ice-covered regions in the south (Fig. 5, *Insets*).

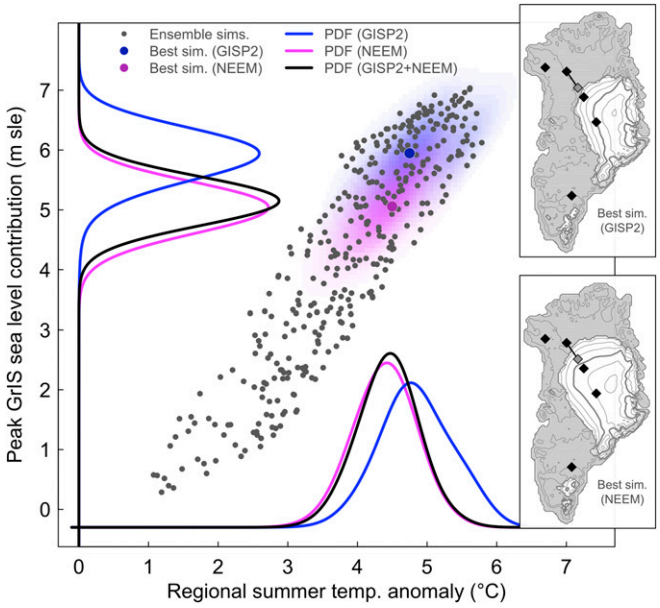

Fig. 5. Simulated maximum GrIS contribution to sea level (m sle) vs. the peak regional summer temperature anomaly (°C) during the Eemian (black points). Background shading shows the 2D marginal probabilities for GISP2 (blue) and NEEM (magenta) estimated using a weighted kernel density estimate. Probabilities projected onto each variable are shown along with the combined (GISP2 + NEEM) estimate. *Insets* show the minimum ice sheet distribution for the best simulation for GISP2 (*Upper*) and NEEM (*Lower*). The black diamonds on the ice sheet indicate drilling sites, and correspond to sites in Fig. 1. The gray diamond connected to the NEEM point is the estimated upstream deposition site for Eemian age ice.

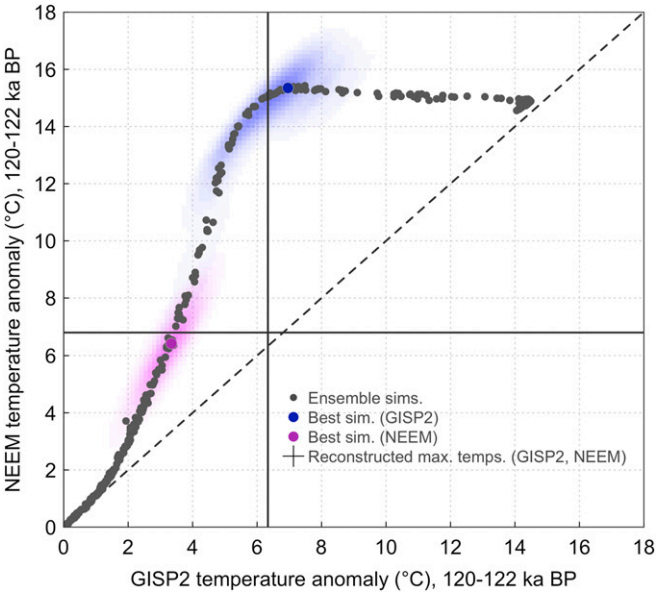

Fig. 6. Simulated average precipitation-weighted temperature anomalies (°C) at NEEM vs. those of GISP2 during the Eemian for the period 120–122 ka BP (black points). Background shading and the colored points shows the 2D marginal probabilities estimated using a weighted kernel density estimate and the optimal simulations, respectively, for GISP2 (blue) and NEEM (magenta), and the cross indicates the corresponding reconstructed temperature anomalies from the ice cores for this time period. For comparison, the 1:1 relationship of temperature anomalies at NEEM vs. GISP2 is shown by the dashed line.

The initial rise in temperature seen in all of the simulations is predominantly due to the background regional warming. These high temperatures initiate melting and a reduction of the volume and area of the ice sheet. Ice dynamics dictate that there must be a lag between the onset of melting and the volume reduction, because the former can only occur at a limited rate. By 125 ka, regional temperatures begin to fall. In the both optimum simulations, Summit and NEEM remain warm until ∼122.5 ka due to declining elevations, which counteract the regional cooling signal (see Fig. S5 for the Summit-optimal case). At around 122–121 ka, the simulated ice volume reaches its minimum, elevations stabilize and the background cooling again dominates the local temperature signal.

There are a number of features that the optimum models fail to capture. First, and most apparent, is the magnitude of the early temperature anomalies of approximately 6–8 °C at both GISP2 and NEEM. This poor fit is in stark contrast to the rather good fit later in the Eemian. It is unlikely that the regional temperature forcing was larger than simulated here, because it would result in even faster ice sheet melt and an even worse overall fit with the reconstructions. Furthermore, the sensitivity of $\delta^{18}O_{ice}$ to temperature may not always be within the range 2.1 ± 0.5 °C/‰. Temporal deviations away from this factor may account for the misfit between inferred and simulated temperature histories early in the Eemian. In general, the use of a constant conversion factor in time could in fact erroneously suggest a constant temperature difference between GISP2 and NEEM and should also be regarded cautiously.

Second, the optimum simulation predicts maximum accumulation rates at GISP2 similar to the Holocene, although the data suggest that rates were considerably higher (Fig. 4 and Fig. S6). Gas-trapping depths (based on the gravitational enrichment of N_2)

are temperature dependent, and they were similar during the Holocene and Eemian. However, Eemian isotopic temperatures were much warmer. Warmer temperatures imply higher accumulation rates to prevent shoaling of the trapping depth. The model does not reproduce the NEEM accumulation rate record well. Thus, it may be that simulated SLR contributions are slightly overestimated as a result of mismatches between inferred and simulated accumulation rates, although the work of Cuffey and Marshall (31) suggest that the bias would be less than ∼0.5 m.

The poor fit with some aspects of the reconstructions may imply that a more detailed modeling approach is needed. The dominant driver of GrIS changes during the Eemian is changes in surface mass balance and, thus, changes in climate. Here we applied a spatially constant temperature anomaly to force our simple regional climate model, which could bias the comparison between the two cores if in reality the climate showed more complex patterns of anomalies. Nonetheless, the overall sensitivity of the ice sheet to large-scale climate changes (as well as its uncertainty) should be well represented by our ensemble of simulations, which gives confidence to the estimated ice sheet retreat and sea level contribution.

Optimizing the Greenland sea level rise (SLR) contribution against both temperature records suggests that the GIS contribution was 5.1 m (4.1–6.2 m; 95% credible interval). Given regional summer temperature anomalies in the range of 3–5 °C, a substantial elevation reduction at both sites is required to achieve and sustain the high Eemian temperatures implied by the $\delta^{18}O_{ice}$ data. If, instead, the minimum elevations at these sites would have been comparable to today, the regional temperature anomaly required to reproduce the $\delta^{18}O_{ice}$ signal would be closer to 8–10 °C (Fig. S5). Such warm values would be inconsistent with other Arctic paleo archives (32), as well as global climate model simulations for the period (33), which show no more than 0.5–6.5 °C summer warming. In addition, summer temperature anomalies of 8–10 °C would melt the GrIS completely in even the most conservative members of the model ensemble. Such a fate would obviously be inconsistent with the existence of Eemian-age ice at the base of the GrIS. Invoking a lower sensitivity of T to $\delta^{18}O_{ice}$, say 1.5°/‰, diminishes the magnitude of the temperature change, but does not change the basic picture.

The data–model comparison reveals a key challenge to our understanding of the climatic reconstructions from the two sites. Both the TAC and $\delta^{18}O_{ice}$ data indicate that changes in elevation and temperature in both cores were similar throughout the Eemian (Figs. 3 and 6). However, the simulations indicate that for only moderate warming at GISP2 of less than 2 °C, the NEEM temperature already becomes significantly higher (Fig. 6). This is not surprising. The NEEM deposition site sits closer to the margin in a rather arid zone of the ice sheet, where a small amount of warming leads to ice loss in the region. Therefore, it is not possible to obtain high enough temperatures to match the GISP2 reconstruction while maintaining low enough temperatures to match the NEEM reconstruction. This apparent paradox could potentially be resolved if the location of the NEEM deposition site changed much more dynamically during the Eemian than has been assumed until now.

Implications for the Source of Last Interglacial Sea Level Rise. Our optimum simulations give a maximum Greenland contribution of 5 and 6 m to Eemian sea level rise, using NEEM and GISP2, respectively. The 95% credible uncertainty interval supports a large contribution from Greenland of at least 3.9 m (based on the more conservative NEEM–optimal comparison), and the joint probability density function (PDF) gives a range of 4.1–6.2 m. This range is considerably higher than most recent estimates (5). Our model includes an explicit representation of the albedo–melt feedback, as well as the effect of changing insolation on surface mass balance, which could explain a greater sensitivity here to Eemian climate changes than seen in previous studies (e.g., 34, 35). Helsen et al. (36) estimate the maximum sea level contribution from Greenland to be between 1.2 and 3.5 m, using a regional climate model coupled to an ice sheet model via a full energy balance model at the surface. Their results are quite consistent with the TAC-based reconstruction of small elevation changes at NEEM during the Eemian (6). However, at both the Summit and at NEEM, their modeled temperature anomaly is underestimated by several degrees compared with the reconstructions. In contrast, we find that the simulations with significant reductions in elevation at both Summit and NEEM are most consistent with the isotopic temperature reconstructions.

According to the data, GISP2 and NEEM initially reach temperatures comparable to preindustrial levels only at ∼127 ka. In the simulations, Greenland first begins contracting below its present volume at ∼126 ka. The maximum Greenland sea level contribution is attained in the most likely simulations at ∼121 ka, just as Greenland temperatures start to fall below preindustrial levels. Meanwhile, according to Dutton et al. (5) and O'Leary et al. (37), global sea level was already elevated by 3–6 m above the modern level at 127 ka. East Antarctica warmed to Holocene temperatures by ∼131 ka, and reached a temperature maximum shortly thereafter (38). Therefore, Antarctica is a much stronger candidate than Greenland as the source of elevated the sea level early in Eemian (see also ref. 38). Our data suggest that Greenland contributed to elevated sea level at the end of the Eemian (∼121 ka) and its maximum contribution was likely not coeval with that of Antarctica.

Finally, at neither Summit nor NEEM do we observe any evidence for a collapse of the GrIS that would correspond to the sea level rise at 120 ka inferred from western Australian coral samples (37). If there was such a collapse its source must have been east or west Antarctica.

Conclusions

We have presented a reconstructed history of temperature, accumulation rate, and elevation change at Summit, Greenland, during the Eemian. The $\delta^{18}O_{ice}$ data from the GISP2 ice core indicate that Summit warmed rapidly through the deglacial, with local, precipitation-weighted temperatures rising to ∼4–8 °C above the modern millennial average between 128 and 126 ka. The local temperature remained high throughout the Eemian until ∼121 ka, even as the regional temperature likely fell because of lower insolation. This sustained plateau in Summit temperature results from the sum of regional temperature and local elevation effects on $\delta^{18}O_{ice}$. Accumulation rates remain high and variable through the early and mid-Eemian at Summit, which contrasts with the steady decline in accumulation rates observed at NEEM. Total air content data indicate that the elevation difference between GISP2 and NEEM remained relatively constant during the Eemian.

In the data and in the simulations, Greenland surpassed its preindustrial temperature at ∼127 ka. Both the data and the simulations suggest that Greenland was not responsible for the elevated global sea level observed at this time. By 121 ka, however, we estimate that the Greenland ice sheet contributed 5.1 m (4.1–6.2 m, 95% credible interval) to excess sea level rise relative to the modern. There is no evidence, however, that Greenland melting contributed to the inferred rapid rise in sea level at 120 ka. Finally, although our results imply a large contribution of Greenland to sea level during this time, discrepancies between the simulated and observed relative changes between the ice cores remain to be explained. In addition, of course, this and similar studies are also limited by the fidelity of the climate and ice sheet models used in the simulations.

Methods

Air Analysis. CH_4 and total air content measurements were conducted at Oregon State University (OSU) following analytical methods detailed in Grachev et al. (39), Mitchell et al. (40), and Rosen et al. (41). Out of 48 samples, we excluded two in which replicate subsamples differed by more than 25 ppb.

We also eliminated five samples with likely excess concentrations of CH_4 (*Results and Discussion*). The SD of replicates for the remaining 41 samples was ±3 ppb. An interlaboratory comparison of Holocene and Younger Dryas CH_4 data shows good agreement and validates comparisons of CH_4 concentrations between the NEEM and NGRIP (analyzed at University of Bern; ref. 6) and GISP2 ice cores (analyzed at OSU). The early Holocene NEEM CH4 average from OSU is ∼736 ppb (41), and from Bern is ∼735 ppb (44). During the Younger Dryas, the NEEM CH_4 average from OSU is 503 ppb; that of Bern is 506 ppb.

$\delta O_2/N_2$, $\delta Ar/N_2$, $\delta^{15}N$, and $\delta^{18}O_{atm}$ of trapped air was measured using an adapted extraction and equilibration technique based on Emerson et al. (42) and Dreyfus et al. (43). In these extractions, ∼20 g of ice were used, and the equilibrating time of the headspace and melt water was 1 h. The analytical uncertainty based on the SDs of modern air standards (air taken directly from the roof of the Princeton University Geosciences building in New Jersey; $n = 28$) for $\delta O_2/N_2$ is ±0.49‰, for $\delta Ar/N_2$ is ±0.29‰, for $\delta^{15}N$ is ±0.02‰, and for $\delta^{18}O$ of O_2 is ±0.04‰. The paleoatmospheric $\delta^{18}O$, $\delta^{18}O_{atm}$, is equal to $\delta^{18}O$ of O_2 corrected for gravitational fractionation: $\delta^{18}O_{atm} = \delta^{18}O - 2.01 * \delta^{15}N$. The SD for $\delta^{18}O_{atm}$ of modern air standards is ±0.04‰.

ACKNOWLEDGMENTS. We thank the members of the National Ice Core Laboratory for their support in recovering samples from the ice core archive. We are grateful to Mahé Perrette for help with the statistical analysis. This work was supported by Grants PLR 1107343 and 1107744 from the U.S. National Science Foundation. A.R. was funded by the Marie Curie Seventh Framework Programme [Project PIEF-GA-2012-331835; European Ice Sheet Modeling Initiative (EURICE)] and the Spanish Ministerio de Economía y Competitividad [Project CGL2014-59384-R; Modeling Abrupt Climate Change (MOCCA)]. M.L.B. was funded by the Princeton-BP Amoco Carbon Mitigation Initiative.

1. Clark PU, Huybers P (2009) Global change: Interglacial and future sea level. *Nature* 462(7275):856–857.
2. Kopp RE, Simons FJ, Mitrovica JX, Maloof AC, Oppenheimer M (2009) Probabilistic assessment of sea level during the last interglacial stage. *Nature* 462(7275):863–867.
3. IPCC (2013) Annex I: Atlas of global and regional climate projections. *Climate Change 2013: The Physical Science Basis. Contribution of Working Group I to the Fifth Assessment Report of the Intergovernmental Panel on Climate Change* eds Stocker TF et al. (Cambridge Univ Press, Cambridge, UK).
4. IPCC (2013) Annex II: Climate system scenario tables. *Climate Change 2013: The Physical Science Basis. Contribution of Working Group I to the Fifth Assessment Report of the Intergovernmental Panel on Climate Change*, eds Stocker TF, et al. (Cambridge Univ Press, Cambridge, UK).
5. Dutton A, et al. (2015) Sea-level rise due to polar ice-sheet mass loss during past warm periods. *Science* 349(6244):aaa4019.
6. NEEM Community Members (2013) Eemian interglacial reconstructed from a Greenland folded ice core. *Nature* 493(7433):489–494.
7. Raynaud D, et al. (2007) The local insolation signature of air content in Antarctic ice. A new step toward an absolute dating of ice records. *Earth Planet Sci Lett* 261(3-4): 337–349.
8. Suwa M, von Fischer JC, Bender ML, Landais A, Brook EJ (2006) Chronology reconstruction for the disturbed bottom section of the GISP2 and the GRIP ice cores: Implications for Termination II in Greenland. *J Geophys Res Atmos* 111, 10.1029/2005JD006032.
9. Chappellaz J, Brook E, Blunier T, Malaize B (1997) CH_4 and delta O-18 of O-2 records from Antarctic and Greenland ice: A clue for stratigraphic disturbance in the bottom part of the Greenland Ice Core Project and the Greenland Ice Sheet Project 2 ice cores. *J Geophys Res Oceans* 102(C12):26547–26557.
10. Grootes PM, Stuiver M, White JWC, Johnsen S, Jouzel J (1993) Comparison of oxygen-isotope records from the GISP2 and GRIP Greenland ice cores. *Nature* 366(6455): 552–554.
11. Johnsen SJ, et al. (2001) Oxygen isotope and palaeotemperature records from six Greenland ice-core stations: Camp Century, Dye-3, GRIP, GISP2, Renland and NorthGRIP. *J Quat Sci* 16(4):299–307.
12. Capron E, et al. (2010) Synchronising EDML and NorthGRIP ice cores using delta O-18 of atmospheric oxygen (delta O-18(atm)) and CH4 measurements over MIS5 (80-123 kyr). *Quat Sci Rev* 29(1-2):222–234.
13. Loulergue L, et al. (2008) Orbital and millennial-scale features of atmospheric CH4 over the past 800,000 years. *Nature* 453(7193):383–386.
14. Dreyfus GB (2008) Dating an 800,000 year Antarctic ice core record using the isotopic composition of trapped air. Thesis dissertation (Princeton University, Princeton, NJ).
15. Robinson A, Calov R, Ganopolski A (2010) An efficient regional energy-moisture balance model for simulation of the Greenland Ice Sheet response to climate change. *Cryosph* 4(2):129–144.
16. Greve R (1997) A continuum–mechanical formulation for shallow polythermal ice sheets. *Philos Trans R Soc London Ser A Math Phys Eng Sci* 355(1726):921–974.
17. Ganopolski A, Calov R (2011) The role of orbital forcing, carbon dioxide and regolith in 100 kyr glacial cycles. *Clim Past* 7(4):1415–1425.
18. Robinson A, Calov R, Ganopolski A (2012) Multistability and critical thresholds of the Greenland ice sheet. *Nat Clim Chang* 2(4):429–432.
19. van de Berg WJ, van den Broeke MR, van Meijgaard E, Kaspar F (2013) Importance of precipitation seasonality for the interpretation of Eemian ice core isotope records from Greenland. *Clim Past* 9(4):1589–1600.
20. Vinther BM, et al. (2009) Holocene thinning of the Greenland ice sheet. *Nature* 461(7262):385–388.
21. Johnsen SJ, Dansgaard W, White JWC (1989) The origin of Arctic precipitation under present and glacial conditions. *Tellus B Chem Phys Meteorol* 41(4):452–468.
22. Merz N, Born A, Raible CC, Fischer H, Stocker TF (2014) Dependence of Eemian Greenland temperature reconstructions on the ice sheet topography. *Clim Past* 10(4): 1221–1238.
23. Sowers T, Bender ML, Raynaud D (1989) Elemental and isotopic composition of occluded O_2 and N_2 in polar ice. *J Geophys Res Atmos* 94(D4):5137–5150.
24. Herron MM, Langway CC (1980) Firn densification – An empirical model. *J Glaciol* 25(93):373–385.
25. Martinerie P, Raynaud D, Etheridge DM, Barnola JM, Mazaudier D (1992) Physical and climatic parameters which influence the air content in polar ice. *Earth Planet Sci Lett* 112(1-4):1–13.
26. Eicher O, et al. (2015) Climatic and insolation control on the high-resolution total air content in the NGRIP ice core. *CIlim. Past Discuss.* 11:5509–5548.
27. Lipenkov V, Raynaud D, Loutre M, Duval P (2011) On the potential of coupling air content and O_2/N_2 from trapped air for establishing an ice core chronology tuned on local insolation. *Quat Sci Rev* 30(23-24):3280–3289.
28. Schilt A, et al. (2010) Atmospheric nitrous oxide during the last 140,000 years. *Earth Planet Sci Lett* 300(1-2):33–43.
29. Buiron D, et al. (2011) TALDICE-1 age scale of the Talos Dome deep ice core, East Antarctica. *Clim Past* 7(1):1–16.
30. Petit JR, et al. (1999) Climate and atmospheric history of the past 420,000 years from the Vostok ice core, Antarctica. *Nature* 399(6735):429–436.
31. Cuffey KM, Marshall SJ (2000) Substantial contribution to sea-level rise during the last interglacial from the Greenland ice sheet. *Nature* 404(6778):591–594.
32. Capron E, et al. (2014) Temporal and spatial structure of multi-millennial temperature changes at high latitudes during the Last Interglacial. *Quat Sci Rev* 103:116–133.
33. Bakker P, et al. (2013) Last interglacial temperature evolution – A model inter-comparison. *Clim Past* 9(2):605–619.
34. Quiquet A, Ritz C, Punge HJ, Salas y Melia D (2013) Greenland contribution to sea level rise during the last glacial period: A modeling study driven and constrained by ice core data. *Clim Past* 9(1):353–366.
35. Stone EJ, Lunt DJ, Annan JD, Hargreaves JC (2013) Quantification of the Greenland ice sheet contribution to Last Interglacial sea level rise. *Clim Past* 9(2):621–639.
36. Helsen MM, van der Berg WJ, van de Wal RSW, van den Broeke MR, Oerlemans J (2013) Coupled regional climate-ice-sheet simulation shows limited Greenland ice loss during the Eemian. *Clim Past* 9(4):1773–1788.
37. O'Leary MJ, et al. (2013) Ice sheet collapse following a prolonged period of stable sea-level during the last interglacial. *Nat Geosci* 6(9):796–800.
38. Steig EJ, et al. (2015) Influence of West Antarctic Ice Sheet collapse on Antarctic surface climate. *Geophys Res Lett* 42(12), 10.1002/2015GL063861.
39. Grachev AM, Brook EJ, Severinghaus JP, Pisias NG (2009) Relative timing and variability of atmospheric methane and GISP2 oxygen isotopes between 68 and 86 ka. *Global Biogeochem Cycles* 23, 10.1029/2008GB003330.
40. Mitchell LE, Brook EJ, Sowers T, McConnell JR, Taylor K (2011) Multidecadal variability of atmospheric methane, 1000-1800 CE. *J Geophys Res Biogeosci* 116, 10.1029/2010JG001441.
41. Rosen JL, et al. (2014) An ice core record of near-synchronous global climate changes at the Bolling transition. *Nat Geosci* 7(6):459–463.
42. Emerson S, Quay PD, Stump C, Wilbur D, Schudlich R (1995) Chemical tracers of productivity and respiration in the subtropical Pacific Ocean. *J Geophys Res Oceans* 100(C8):15873–15887.
43. Dreyfus GB, et al. (2007) Anomalous flow below 2700 m in the EPICA Dome C ice core detected using delta O-18 of atmospheric oxygen measurements. *Clim Past* 3(2): 341–353.
44. Baumgartner M, et al. (2012) High-resolution interpolar difference of atmospheric methane around the Last Glacial Maximum. *Biogeosciences* 9(11):3961–3977.
45. Bender ML, Sowers T, Lipenkov V (1995) On the concentrations of O-2, N-2, and Ar in trapped gases from ice cores. *J Geophys Res Atmos* 100(D9):18651–18660.
46. Bender ML, Burgess E, Alley RB, Barnett B, Clow GD (2010) On the nature of the dirty ice at the bottom of the GISP2 ice core. *Earth Planet Sci Lett* 299(3-4):466–473.
47. Souchez R, Janssens L, Lemmens M, Stauffer B (1995) Very-low oxygen concentration in basal ice from Summit, Central Greenland. *Geophys Res Lett* 22(15):2001–2004.
48. Seierstadt I, et al. (2014) Consistently dated records from the Greenland GRIP, GISP2 and NGRIP ice cores for the past 104 ka reveal regional millennial-scale $\delta^{18}O$ gradients with possible Heinrich event imprint. *Quat Sci Rev* 106:29–46.
49. Raynaud D, Chappellaz J, Ritz C, Martinerie P (1997) Air content along the Greenland Ice Core Project core: A record of surface climatic parameters and elevation in central Greenland. *J Geophys Res Oceans* 102(C12):26607–26613.
50. Martinerie P, et al. (1994) Air content paleo record in the Vostok ice core (Antarctica): A mixed record of climatic and glaciological parameters. *J Geophys Res* 99(D5): 10565–10576.